A&A 602, L3 (2017)
DOI: 10.1051/0004-6361/201629792


Astronomy & Astrophysics

Letter to the Editor

# Gas versus solid-phase deuterated chemistry: HDCO and $D_2CO$ in massive star-forming regions

S. Zahorecz[1,2,3,4,5], I. Jimenez-Serra[6], L. Testi[4,7,9], K. Immer[4], F. Fontani[7], P. Caselli[8], K. Wang[4], and L. V. Toth[5]

[1] Department of Physical Science, Graduate School of Science, Osaka Prefecture University, 1-1 Gakuen-cho, Naka-ku, Sakai, Osaka 599-8531, Japan
e-mail: s.zahorecz@p.s.osakafu-u.ac.jp
[2] National Astronomical Observatory of Japan, National Institutes of Natural Science, 2-21-1 Osawa, Mitaka, 181-8588 Tokyo, Japan
[3] Konkoly Observatory, Research Centre for Astronomy and Earth Sciences, Hungarian Academy of Sciences, 1121 Budapest, Konkoly Thege Miklós út 15–17, Hungary,
[4] European Southern Observatory, Karl-Schwarzschild-Str. 2, 85748 Garching bei München, Germany
[5] Eötvös Loránd University, Department of Astronomy, Pázmány Péter sétány 1/A, 1117 Budapest, Hungary
[6] School of Physics and Astronomy, Queen Mary University of London, Mile End Road, E1 4NS London, UK
[7] INAF-Osservatorio Astrofisico di Arcetri, L.go E. Fermi 5, 50125 Firenze, Italy
[8] Max-Planck-Institut für Extraterrestrische Physik, Giessenbachstrasse 1, 85748 Garching bei München, Germany
[9] Excellence Cluster Universe, Boltzmannstr. 2, 85748 Garching bei München, Germany

Received 27 September 2016 / Accepted 8 May 2017

**ABSTRACT**

*Context.* The formation of deuterated molecules is favoured at low temperatures and high densities. Therefore, the deuteration fraction ($D_{\rm frac}$) is expected to be enhanced in cold, dense prestellar cores and to decrease after protostellar birth. Previous studies have shown that the deuterated forms of species such as $N_2H^+$ (formed in the gas phase) and $CH_3OH$ (formed on grain surfaces) can be used as evolutionary indicators and to constrain their dominant formation processes and timescales.
*Aims.* Formaldehyde ($H_2CO$) and its deuterated forms can be produced both in the gas phase and on grain surfaces. However, the relative importance of these two chemical pathways is unclear. Comparison of the deuteration fraction of $H_2CO$ with respect to that of $N_2H^+$, $NH_3$, and $CH_3OH$ can help us to understand its formation processes and timescales.
*Methods.* With the new SEPIA Band 5 receiver on APEX, we have observed the $J = 3 \rightarrow 2$ rotational lines of HDCO and $D_2CO$ at 193 GHz and 175 GHz toward three massive star-forming regions hosting objects at different evolutionary stages: two high-mass starless cores (HMSC), two high-mass protostellar objects (HMPOs), and one ultracompact HII region (UC HII). By using previously obtained $H_2CO$ $J = 3 \rightarrow 2$ data, the deuteration fractions HDCO/$H_2CO$ and $D_2CO$/HDCO are estimated.
*Results.* Our observations show that singly deuterated $H_2CO$ is detected toward all sources and that the deuteration fraction of $H_2CO$ increases from the HMSC to the HMPO phase and then sharply decreases in the latest evolutionary stage (UCHII). The doubly deuterated form of $H_2CO$ is detected only in the earlier evolutionary stages, with $D_2CO/H_2CO$ showing a pattern that is qualitatively consistent with the pattern of HDCO/$H_2CO$, within current uncertainties.
*Conclusions.* Our initial results show that $H_2CO$ may display a similar $D_{\rm frac}$ pattern as that of $CH_3OH$ in massive young stellar objects. This finding suggests that solid-state reactions dominate its formation.

**Key words.** astrochemistry – ISM: molecules – stars: formation – radio lines: ISM

## 1. Introduction

In molecular cloud cores, the formation of deuterated molecules is favoured at low temperatures ($T \leq 20$ K) and at high densities ($n \geq 10^4$ cm$^{-3}$). It is thus expected that the deuteration fraction ($D_{\rm frac}$, the relative abundance between a species containing $D$ as compared to the same species containing H) is enhanced in cold and dense prestellar cores. $D_{\rm frac}$ should then decrease after protostellar birth, when the young stellar object heats the central region of the core (Caselli 2002). For low-mass star-forming cores, observations of deuterated species produced in gas-phase reactions, such as $H_2D^+$ and $N_2D^+$, have confirmed this theoretical scenario (Crapsi et al. 2005; Caselli et al. 2008).

Recent studies show that high $D_{\rm frac}$ values are also typical for high-mass star-forming cores and that the $D_{\rm frac}$ of some species could also be an evolutionary indicator in the intermediate- and high-mass regime (e.g. Busquet et al. 2010; Fontani et al. 2011; Sakai et al. 2012). High-mass star-forming regions can be divided into the following evolutionary stages: high-mass starless cores (HMSCs), high-mass protostellar objects (HMPOs), and ultracompact HII regions (UCHIIs; e.g. Beuther et al. 2007; Tan et al. 2014). By studying several deuterated species in 27 massive cores, Fontani et al. (2011, 2015) found that species formed exclusively in the gas ($N_2H^+$) showed different evolutionary trends from those formed partially ($NH_3$) or totally ($CH_3OH$) on grain mantles. The abundance of $N_2D^+$ is indeed higher in HMSCs, and it drops by about an order of magnitude during the HMPO and UCHII stages. This is due to the higher gas temperatures found in the latter objects, which allow the destruction of $H_2D^+$ via the endothermic reaction $H_2D^+ + H_2 \rightarrow H_3^+ + HD$ (see Gerlich et al. 2002; Fontani et al. 2011). In contrast, deuterated methanol, formed only on grain surfaces, is detected towards HMPOs and externally heated HMSCs only, possibly as a result of evaporation or sputtering of grain mantles. Therefore, while $D_{\rm frac}(N_2H^+)$ can be used as an indicator of the initial conditions in starless or pre-stellar cores, high values of $D_{\rm frac}(CH_3OH)$ are a good probe of the earliest protostellar phases (Fontani et al. 2015). The deuteration fraction of $NH_3$, whose

formation pathways occur both in the gas-phase and on grain surfaces, does not show statistically significant changes with evolution, and therefore there is no dominant formation pathway for $NH_3$ and its deuterated forms.

Like $NH_3$, formaldehyde ($H_2CO$) may also be produced both in the gas phase and on grain surfaces. The two main pathways for the production of $H_2CO$ (and its deuterated counterparts) involve $CH_3^+$ (viz. $CH_2D^+$ and $CHD_2^+$) in the gas phase and multiple hydrogenation (viz. deuteration) of CO in the ices (see e.g. Roberts & Millar 2007). The gas phase pathway is similar to the one of $N_2H^+$ with the main difference that deuteration of $H_2CO$ can also occur at warmer temperatures (30−50 K, see Parise et al. 2009), whereas $T < 20$ K are needed to increase the deuteration of $N_2H^+$ via $H_2D^+$. The ice phase formation route of $H_2CO$ is similar to that of $CH_3OH$ and their deuterated forms. Although laboratory work and observational studies of low-mass protostars suggests an important contribution from grain surface chemistry for the production of $H_2CO$ (Watanabe 2005; Roberts & Millar 2007; Bergman et al. 2011), the relative importance of the dust grain vs. gas-phase formation routes remains unclear. Furthermore, $D_2CO$ measurements in intermediate- and in high-mass star-forming regions are lacking ($D_2CO$ has been firmly detected toward NGC 7129-FIRS 2 and tentatively toward the MonR2 ultra-compact HII region; Fuente et al. 2005; Treviño-Morales et al. 2014), and it is thus unknown whether the chemistry of $H_2CO$ and of its deuterated counterparts is governed by the same mechanisms in both low-mass and more massive objects.

In this Letter, we report the first detection of doubly deuterated formaldehyde, $D_2CO$, toward high-mass star-forming cores. These are the initial findings of a search for HDCO and $D_2CO$ emission toward three high-mass star-forming regions at different evolutionary stages using the new SEPIA Band 5 receiver available at the Atacama Pathfinder EXperiment (APEX[1]) telescope. The targets were extracted from the sample of Fontani et al. (2011), for which the deuteration fraction of other molecules (e.g. $N_2H^+$, $CH_3OH$, and $NH_3$) has been measured (Fontani et al. 2015). The evolutionary stages of our sample reach from the initial conditions in HMSCs to the HMPOs phase and the UCHII regions. The source sample and the observations are described in Sect. 2, while our results are presented in Sect. 3. In Sect. 4 we discuss our results and place them in context with respect to previous findings in low-mass star-forming regions. In Sect. 5 we summarize our conclusions.

## 2. Observations

### 2.1. Selected targets

The selected sources are extracted from Fontani et al. (2011) and are AFGL5142, IRAS 05358+3543, and G5.89-0.39. These are the sources with the brightest lines of $H_2CO$ within each evolutionary stage. We note that this selection may introduce biases, therefore a follow-up study with a larger sample is needed. The bolometric luminosities of the objects are $10^{3.6}$, $10^{3.8}$, and $10^{5.1}$ $L_\odot$ and the integrated gas masses are 210, 300, and 300 $M_\odot$ for AFGL5142, IRAS 05358, and G5.89, respectively (Fontani et al. 2011; Liu et al. 2016; Beuther et al. 2002b, 2005; Tang et al. 2009). AFGL5142 is a high-mass star-forming region (distance of 2.14 ± 0.05 kpc; Burns et al., in prep.) that hosts several dense cores at different evolutionary stages: the central core (CC, classified as an HMPO), the western core (WC, an HMSC core), and the eastern core (EC; see Busquet et al. 2011; Fontani et al. 2011). We centred our single-pointing observations on CC. However, because the separation between WC and CC is 9″ and because the APEX beam is ∼34″ at 190 GHz, WC and CC were also covered in our observations. The $N_2H^+$ (1−0) emission in AFGL5142 shows two velocity components at −2 and −4 km s$^{-1}$, associated with CC and WC, respectively (Busquet et al. 2011).

IRAS 05358+3543, located at 1.8 kpc (Snell et al. 1990), contains three dust condensations (mm1, mm2, and mm3) within an area of 9″ × 4″ (Beuther et al. 2002a). According to Leurini et al. (2007), mm1 splits into mm1a, a hot core and a massive circumstellar disk with $T \sim 220$ K, and mm1b, which is at an earlier stage of evolution. Source mm2 is a low-to-intermediate mass protostar, while mm3 is an HMSC. Our observation is centred on mm1, but all three dust condensations are covered within the APEX beam.

G5.89-0.39 is a shell-like UCHII region (diameter of ∼4″) found at $2.99^{+0.19}_{-0.17}$ kpc (Sato et al. 2014). Sub-arcsecond observations reveal at least five dust condensations (Su et al. 2009). We centred our observations on the SMA-N dust condensation. Several energetic outflows and maser activity have been detected toward G5.89-0.39 (see e.g. Hunter et al. 2008; Fish et al. 2005).

### 2.2. IRAM-30 m $H_2CO$ observations

Previous observations of these objects were performed using the IRAM-30 m telescope (details can be found in Fontani et al. 2011, 2015). The frequency setups included the $3_{03}$−$2_{02}$, $3_{22}$−$2_{21}$, and $3_{21}$−$2_{20}$ transitions of $H_2CO$. The spectroscopic information of these transitions is shown in Table A.1 (Müller et al. 2005). The $H_2CO$ line emission is very strong in all three sources, with a measured $T_{MB} > 5$ K (top panels in Fig. A.1).

### 2.3. APEX SEPIA observations

The three sources were observed with the APEX SEPIA receiver (Swedish-ESO PI receiver for APEX; Billade et al. 2012)[2]. We carried out single-pointing observations of HDCO and $D_2CO$ using the position-switching observing mode. The J2000 central coordinates used in our observations were [RA, Dec] = (05:30:48.0, +33:47:54) for AFGL5142, [RA, Dec] = (05:39:13.0, +35:45:51) for IRAS05358+3543, and [RA, Dec] = (18:00:30.5, −24:04:01) for G5.89-0.39. The observed transitions of HDCO (at 185 GHz and 193 GHz) and $D_2CO$ (at 174.4 GHz) are shown in Table A.1. The pointing was checked every 60−90 min, and the typical system temperatures were 150 K. The beam size at 183 GHz was ∼34″ and a beam efficiency of 0.83 was used. The XFFTS spectrometer provided a velocity resolution of 0.059 km s$^{-1}$ and 0.066 km s$^{-1}$ for the HDCO (at 185−193 GHz) and $D_2CO$ transitions (at 174 GHz), respectively. However, for the data analysis, we smoothed the spectra to a uniform velocity resolution of 0.5 km s$^{-1}$. At this velocity resolution, we reached an rms of ∼0.01 K with typical integration times between 32 and 48 min. The PWV was 0.3−1.5 mm. The data were reduced and analysed with the Gildas software[3] (version jul14a, Pety 2005) and the derived parameters of the detected lines are reported in Appendix A.

[1] This publication is based on data acquired with the Atacama Pathfinder Experiment (APEX). APEX is a collaboration between the Max-Planck-Institut für Radioastronomie, the European Southern Observatory, and the Onsala Space Observatory.

[2] Observations were done as part of Science Verification in July 2015 (project E-095.F-9808A), and in November−October 2015 and May−June 2016 within projects E-096.C-0484A and E097.C-0897A.

[3] See http://www.iram.fr/IRAMFR/GILDAS

**Table 1.** Calculated column densities and ratios (deuteration fractions) for the three species.

| Name | Type | N($H_2CO$) ($10^{13}$ cm$^{-2}$) | N(HDCO) ($10^{13}$ cm$^{-2}$) | N($D_2CO$) ($10^{13}$ cm$^{-2}$) | N(HDCO)/N($H_2CO$) | N($D_2CO$)/N($H_2CO$) | N($D_2CO$)/N(HDCO) |
|---|---|---|---|---|---|---|---|
| AFGL5142 | HMSC | 317 (10) | 11 (3) | 3.4 (2) | 0.035 (0.01) | 0.011 (0.01) | 0.31 (0.3) |
| IRAS 05358+3543 | HMSC/HMPO | >130 (2) | 13.0 (1.4) | 2.6 (1.7) | <0.10 (0.01) | <0.020 (0.01) | 0.20 (0.2) |
| AFGL5142 | HMPO | 40 (2) | 14 (3) | 2.5 (1.6) | 0.34 (0.09) | 0.063 (0.04) | 0.18 (0.15) |
| G5.89-0.39 | UCHII | 1740 (170) | 25 (2) | <2 | 0.014 (0.002) | <0.001 | <0.08 |

**Notes.** The errors for the calculated column density values are the formal fit uncertainties from the least-squares fits performed by MADCUBAIJ. Systematic uncertainties dominate the formal fit uncertainties, see Sect. 3, paragraph 5. Calculated values based on the two velocity components of AFGL5142, corresponding to the previously identified HMSC and HMPO objects by Busquet et al. (2011), are shown separately.

## 3. Results

In Fig. A.1 we present the HDCO and $D_2CO$ lines observed toward AFGL5142, IRAS 05358+3543, and G5.89-0.39. The $H_2CO$ $3_{0,3}-2_{0,2}$ data obtained with the IRAM 30 m observation are also shown for comparison. While the HDCO lines (upper energy levels of 18.5−50.4 K) are clearly detected in all sources with peak intensities ≥35 mK, the $D_2CO$ $3_{0,3}-2_{0,2}$ transition is only observed toward AFGL5142 and IRAS 05358+3543, that is, at the earlier HMSC/HMPO stages. The $3\sigma$ upper limit measured for the $D_2CO$ $3_{2,2}-2_{2,1}$ line toward G5.89-0.39 is ≤6 mK.

In Table A.2 we report the derived parameters of the observed lines of $H_2CO$, HDCO, and $D_2CO$. For AFGL5142, the $D_2CO$ $3_{0,3}-2_{0,2}$ transition shows two velocity components at −2.077 km s$^{-1}$ and −3.658 km s$^{-1}$ (see Table A.2). We thus fitted the entire observed $H_2CO$, HDCO, and $D_2CO$ line emission using two Gaussian line profiles with fixed central velocities at −2.077 km s$^{-1}$ and −3.658 km s$^{-1}$. These two velocity components are associated with the WC core at the HMSC stage (radial velocity ∼−3.5 km s$^{-1}$), and with the CC core at the HMPO stage (at ∼−2 km s$^{-1}$; Busquet et al. 2011). Both cores lie within the single-dish beam of our IRAM 30 m and APEX observations (WC and CC are separated by 9″, while the IRAM 30 m and APEX beam sizes are 11″ and 34″, respectively).

Since the $H_2CO$, HDCO, and $D_2CO$ lines toward G5.89-0.39 show a slight asymmetry in their line profiles, we also fitted these data using two Gaussian line profiles centred at 8.5 and 11.5 km s$^{-1}$. These two components can also be seen in the emission from $N_2H^+$ or $NH_3$, for example (see Fontani et al. 2011, 2015).

For IRAS 05358+3543, $H_2CO$, HDCO and $D_2CO$ show only one velocity component that peaks at −16 km s$^{-1}$.

To estimate the molecular column densities of $H_2CO$, HDCO, and $D_2CO$, we used the MADCUBAIJ software that assumes LTE conditions (Martín et al. 2011; Rivilla et al. 2016). We adopted a source size of 6.″0 as measured from $NH_3$(2, 2) and following Fontani et al. (2015). This source size is consistent with the size obtained in other high-density tracers such as $N_2H^+$(1-0) and $C^{34}S$(7-6) (see Hunter et al. 2008; Busquet et al. 2011). We have attempted to derive the excitation temperature of the gas, $T_{ex}$, using the four APEX HDCO transitions (Table A.1). Most of the observed $J = 3 \rightarrow 2$ lines of $H_2CO$, HDCO, and $D_2CO$ most likely trace gas with similar physical conditions given that their $E_{up}$ and $A_{ij}$ are similar. Hence, the determination of $T_{ex}$ is highly uncertain because only few lines are available. We thus assumed a $T_{ex}$ of 28 K, which is the average temperature obtained from $NH_3$ for IRAS 05358+3545 and AFGL5142 (Fontani et al. 2011)[4]. We note that the assumed value of $T_{ex}$ can change the derived column densities, but not their ratios. When we assume a $T_{ex}$ value in the 20−40 K range, the variation of the column density values compared to the $T_{ex}$ = 28 K case is below 50%. Lower and higher excitation temperatures cannot fit the observed transitions properly. We also estimated the column densities with different source sizes. With a source size of 2″ we cannot fit the observed transitions properly because of optical depth effects. The estimated column densities decrease by factors of 2−3 for a source size of 10”. For AFGL5142, we obtained the $H_2CO$, HDCO, and $D_2CO$ column densities for the velocity components at −2.077 km s$^{-1}$ (CC, in the HMPO stage) and at −3.658 km s$^{-1}$ (WC in the HMSC phase). In Table 1 we report the calculated column densities of $H_2CO$, HDCO, and $D_2CO$ and the deuteration fractions obtained from the column density ratios HDCO/$H_2CO$, $D_2CO$/$H_2CO$, and $D_2CO$/HDCO.

The $H_2^{13}CO$ $3_{1,3}-2_{1,2}$ transition was covered within our APEX SEPIA setup. We have estimated the $H_2CO$ column densities from the $H_2^{13}CO$ column density and using the $^{12}C/^{13}C$ ratio derived by Milam et al. (2005) as a function of Galactocentric distance. The $H_2CO$ lines in AFGL5142 and G5.89-0.39 are not very optically thick since the $H_2CO$ column densities calculated using the main isotopologue $H_2CO$ and the $^{13}C$ isotopologue $H_2^{13}CO$ differ only by factors 0.4 and 3.6. For IRAS 05358+3543, however, the column densities derived from $H_2CO$ and $H_2^{13}CO$ differ by a factor of 9. In this case, we use the column density derived directly from the $H_2CO$ lines and consider it as a lower limit for IRAS 05358.

## 4. Discussion

As proposed by Fontani et al. (2011, 2015), the different trends observed for $D_{frac}(N_2H^+)$, $D_{frac}(CH_3OH)$, and $D_{frac}(NH_3)$ as a function of evolution in high-mass star-forming regions are likely due to the way deuteration occurs for the different species: in the gas phase for $N_2H^+$, on the grain surface for $CH_3OH$, and via a mixture of the two for $NH_3$. For $H_2CO$, $D_2CO$ is expected to be a product of material processed on solid ices since its formation timescales are longer than the depletion timescales in the pre-stellar phase (see Taquet et al. 2012). Consequently, $D_2CO$ should show an evolutionary trend similar to that derived for $D_{frac}(CH_3OH)$, which peaks at the HMPO phase (Fontani et al. 2015). If HDCO were to show a similar behaviour to $D_2CO$, we could conclude that HDCO also forms mostly on dust grains. This hypothesis would be supported by the fact that HDCO is detected in hot cores and hot corinos, while $N_2D^+$ (only formed in the gas phase) is not (see e.g. Fuente et al. 2005).

Although our sample and statistics are limited, our results show a trend for the deuteration fractions HDCO/$H_2CO$ and $D_2CO$/$H_2CO$ to progressively increase from the HMSC to the HMPO stage by factors ∼3−10, and to subsequently decrease at the UCHII phase (by factors ≥20; see Fig. 1). This behaviour is similar to the trend observed for $D_{frac}(CH_3OH)$, and since

[4] Fontani et al. (2011) do not report any temperature for G5.89-0.39 and therefore we assume the same $T_{ex}$ of 28 K for this source.

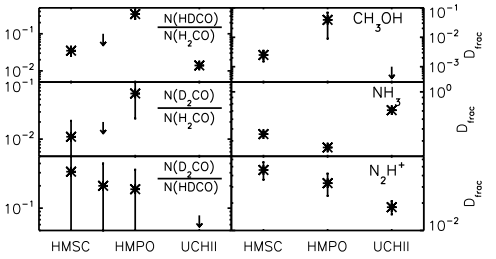


**Fig. 1.** Comparison of the average deuterated fraction of $H_2CO$, HDCO, $CH_3OH$, $NH_3$, and $N_2H^+$. The upper limit for G5.89-0.39 is not shown in the left middle panel, the value is <0.001. Average values for $CH_3OH$, $NH_3$, and $N_2H^+$ based on Fontani et al. (2015) are shown.

the measured HDCO/$H_2CO$ are similar and $D_2CO/H_2CO$ ratios are 4−21 times higher than those predicted by Roberts & Millar (2007) for the production of HDCO and $D_2CO$ via gas-phase reactions, surface chemistry very likely plays an important role in the formation of HDCO and $D_2CO$.

Rodgers & Charnley (2002) indeed proposed a grain surface formation scenario for these molecules in which $H_2CO$ and its deuterated forms represent intermediate steps in the formation of $CH_3OH$ and deuterated-$CH_3OH$ via hydrogenation and D-addition reactions. The extent to which surface chemistry is responsible for the production of HDCO and $D_2CO$ in these sources can be estimated by using the F parameter,

$$F = \frac{[\mathrm{HDCO/H_2CO}]^2}{[\mathrm{D_2CO/H_2CO}]}. \quad (1)$$

From the HDCO/$H_2CO$ and $D_2CO/H_2CO$ ratios in Table 1, we find that $F \sim 0.1$−$0.5$ for HMSCs, $F \sim 1.8$ for HMPOs and $F \geq 0.2$ for UCHIIs. As explained by Rodgers & Charnley (2002), low $F$ values are consistent with grain surface chemistry. However, F values in the range 1.6−2.3 could also be explained by gas-phase chemistry. At the HMPO stage we therefore cannot rule out a contribution to the HDCO/$D_2CO$ production via the gas phase neutral-neutral reactions $CH_2D + O \rightarrow HDCO + H$ and $CHD_2 + O \rightarrow D_2CO + H$. Note that these reactions occur in the forward direction at temperatures ∼30−50 K because the formation reactions of $CH_2D$ and $CHD_2$ are exothermic (Turner 1990).

Table 1 also shows that the $D_2CO$/HDCO ratio remains constant at ∼0.2 within the uncertainties, regardless of the source or evolutionary stage. As for the low-mass regime, the ratio HDCO/$D_2CO$ lies well below the statistical value given as D-species/$D_2$-species = 4 × (D-species/H-species)$^{-1}$, consistent with the grain surface formation scenario (see Ceccarelli et al. 2014).

When we compare the HDCO/$H_2CO$ and $D_2CO/H_2CO$ ratios from Table 1 with those collected by Ceccarelli et al. (2014) for low-mass star-forming regions (see their Fig. 5), we find that the ratio $\frac{\mathrm{HDCO/H_2CO}}{\mathrm{D_2CO/H_2CO}} \sim 3$−$5$ in the high-mass regime, while the same ratio is close to 1 in low-mass star-forming regions. This may be a consequence of the shorter timescales available in the high-mass regime for the formation of $D_2CO$ in the ices (Taquet et al. 2012; Rodgers & Charnley 2002). In the scheme of Rodgers & Charnley (2002), $D_2CO$ is formed after HDCO through two hydrogen-deuterium exchanges experienced by $H_2CO$ in the ices. The higher $\frac{\mathrm{HDCO/H_2CO}}{\mathrm{D_2CO/H_2CO}}$ ratio in high-mass star-forming regions therefore suggests that HDCO may not have had enough time to have been converted into $D_2CO$ as a consequence of the faster evolution of high-mass protostars as compared to their low-mass counterparts.

## 5. Summary

We have observed HDCO and $D_2CO$ toward a sample of high-mass star-forming regions at different evolutionary stages. HDCO transitions were detected for all of them, while the $D_2CO$ line was detected only for the earlier HMSC and HMPO stages. Our results point toward the idea that $H_2CO$ and its deuterated species form mostly on grain surfaces, although some gas-phase contribution is expected at the warm HMPO stage. Interferometric observations are needed to separate the HDCO and $D_2CO$ emission originating from the small and dense cores and to distinguish their origin in high-mass star-forming regions.

*Acknowledgements.* We would like to thank the SEPIA team and APEX team for the successful commissioning of the instrument and for the observations. This work was partly supported by the Gothenburg Centre of Advanced Studies in Science and Technology through the program *Origins of habitable planets* and by the Italian Ministero dell'Istruzione, Università e Ricerca through the grant Progetti Premiali 2012 – iALMA (CUP C52I13000140001) and by NAOJ ALMA Scientific Research Grant Number 2016-03B. K.W. acknowledges the support from Deutsche Forschungsgemeinschaft (DFG) grant WA3628-1/1 through priority programme 1573 ("Physics of the Interstellar Medium"). I.J.-S. acknowledges the financial support received from the STFC through an Ernest Rutherford Fellowship (proposal number ST/L004801/1). L.V.T. and S.Z. acknowledge the support by the OTKA grants NN-111016 and K101393.

## References

Bergman, P., Parise, B., Liseau, R., & Larsson, B. 2011, A&A, 527, A39
Beuther, H., Churchwell, E. B., McKee, C. F., & Tan, J. C. 2007, Protostars and Planets V, 165
Beuther, H., Schilke, P., Gueth, F., et al. 2002a, A&A, 387, 931
Beuther, H., Schilke, P., Menten, K. M., et al. 2002b, ApJ, 566, 945
Beuther, H., Schilke, P., Menten, K. M., et al. 2005, ApJ, 633, 535
Billade, B., Nystrom, O., Meledin, D., et al. 2012, IEEE Trans. Terahertz Sci. Tech., 2, 208
Busquet, G., Estalella, R., Zhang, Q., et al. 2011, A&A, 525, A141
Busquet, G., Palau, A., Estalella, R., et al. 2010, A&A, 517, L6
Caselli, P. 2002, Planet. Space Sci., 50, 1133
Caselli, P., Vastel, C., Ceccarelli, C., et al. 2008, A&A, 492, 703
Ceccarelli, C., Caselli, P., Bockelée-Morvan, D., et al. 2014, Protostars and Planets VI, 859
Crapsi, A., Caselli, P., Walmsley, C. M., et al. 2005, ApJ, 619, 379
Fish, V. L., Reid, M. J., Argon, A. L., & Zheng, X.-W. 2005, ApJS, 160, 220
Fontani, F., Palau, A., Caselli, P., et al. 2011, A&A, 529, L7
Fontani, F., Busquet, G., Palau, A., et al. 2015, A&A, 575, A87
Fuente, A., Neri, R., & Caselli, P. 2005, A&A, 444, 481
Gerlich, D., Herbst, E., & Roueff, E. 2002, Planet. Space Sci., 50, 1275
Hunter, T. R., Brogan, C. L., Indebetouw, R., & Cyganowski, C. J. 2008, ApJ, 680, 1271
Leurini, S., Beuther, H., Schilke, P., et al. 2007, A&A, 475, 925
Liu, T., Zhang, Q., Kim, K.-T., et al. 2016, ApJ, 824, 31
Martín, S., Krips, M., Martín-Pintado, J., et al. 2011, A&A, 527, A36
Milam, S. N., Savage, C., Brewster, M. A., Ziurys, L. M., & Wyckoff, S. 2005, ApJ, 634, 1126
Müller, H. S. P., Schlöder, F., Stutzki, J., & Winnewisser, G. 2005, J. Mol. Struct., 742, 215
Parise, B., Leurini, S., Schilke, P., et al. 2009, A&A, 508, 737
Pety, J. 2005, in SF2A-2005: Semaine de l'Astrophysique Française, eds. F. Casoli, T. Contini, J. M. Hameury, & L. Pagani, 721
Rivilla, V. M., Fontani, F., Beltrán, M. T., et al. 2016, ApJ, 826, 161
Roberts, H. & Millar, T. J. 2007, A&A, 471, 849
Rodgers, S. D. & Charnley, S. B. 2002, Planet. Space Sci., 50, 1125
Sakai, T., Sakai, N., Furuya, K., et al. 2012, ApJ, 747, 140
Sato, M., Wu, Y. W., Immer, K., et al. 2014, ApJ, 793, 72
Snell, R. L., Dickman, R. L., & Huang, Y.-L. 1990, ApJ, 352, 139
Su, Y.-N., Liu, S.-Y., Wang, K.-S., Chen, Y.-H., & Chen, H.-R. 2009, ApJ, 704, L5
Tan, J. C., Beltrán, M. T., Caselli, P., et al. 2014, Protostars and Planets VI, 149
Tang, Y.-W., Ho, P. T. P., Girart, J. M., et al. 2009, ApJ, 695, 1399
Taquet, V., Ceccarelli, C., & Kahane, C. 2012, ApJ, 748, L3
Treviño-Morales, S. P., Pilleri, P., Fuente, A., et al. 2014, A&A, 569, A19
Turner, B. E. 1990, ApJ, 362, L29
Watanabe, N. 2005, in Astrochemistry: Recent Successes and Current Challenges, eds. D. C. Lis, G. A. Blake, & E. Herbst, IAU Symp., 231, 415

## Appendix A: Observed $H_2CO$, HDCO, and $D_2CO$ lines

In Table A.1 we report the parameters of the observed lines for $H_2CO$, HDCO, and $D_2CO$. The observing setup (and the observations of Fontani et al. 2011, 2015) also covered other higher excitation lines of the same molecules, but these were not detected (and are not expected to be detectable under the expected excitation conditions).

In Fig. A.1 we present the HDCO and $D_2CO$ lines observed toward AFGL5142, IRAS 05358+3543, and G5.89-0.39. The $H_2CO$ $3_{0,3}-2_{0,2}$ data obtained with the IRAM 30 m observation are also shown for comparison. While the HDCO lines (upper energy levels of 18.5-50.4 K) are clearly detected in all sources with peak intensities ≥35 mK, the $D_2CO$ $3_{0,3}-2_{0,2}$ transition is only observed toward AFGL5142 and IRAS 05358+3543, that is to say, at the earlier HMSC/HMPO stages. The $3\sigma$ upper limit measured for the $D_2CO$ $3_{2,2}-2_{2,1}$ line toward G5.89-0.39 is ≤6 mK.

In Table A.2 we report the parameters derived by fitting single or multiple (in the case of AFGL5142 and G5.89-0.39) Gaussian profiles to the detected lines. For the HDCO, $H_2^{13}CO$, and $H_2CO$ spectra of AFGL5142 and IRAS 05358+3543, we fitted the $v_{LSR}$ and FWHM values based on the $D_2CO$ velocity components. For G5.89-0.39, we derived the velocity and width of the two components based on the HDCO $3_{0,3} \rightarrow 2_{0,2}$ line. We did not use these fits directly to calculate the physical parameters. We used the velocities and line widths as initial parameters for the MADCUBAIJ modelling.

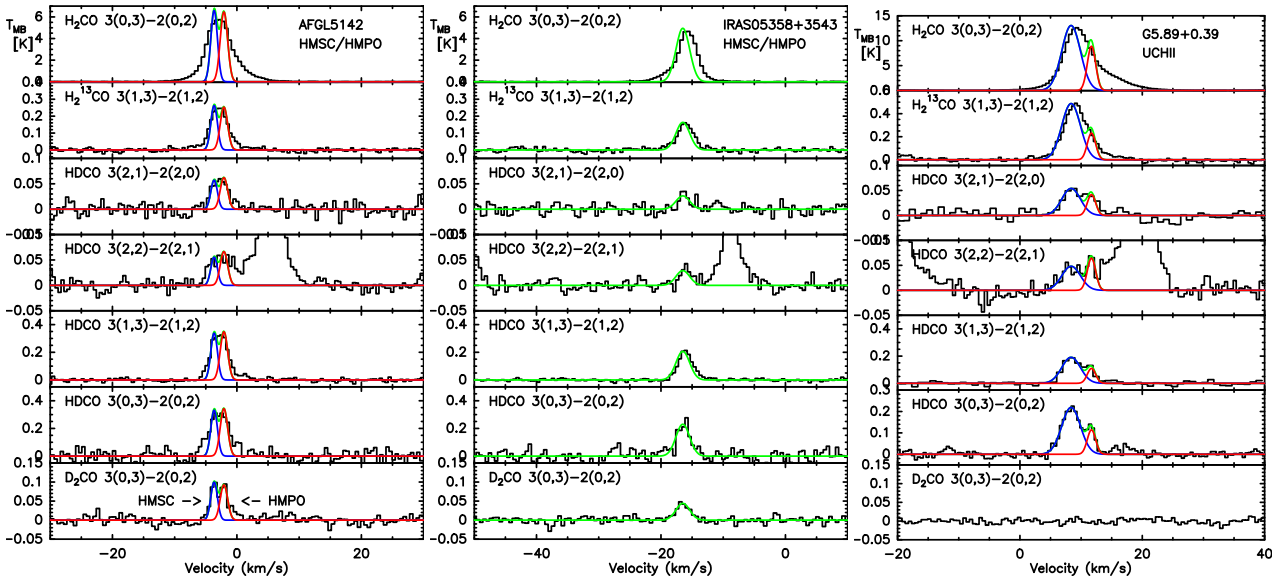


**Fig. A.1.** *From left to right*: spectra of $H_2CO$ $3_{0,3}-2_{0,2}$, $H_2^{13}CO$ $3_{1,3}-2_{1,2}$, HDCO $3_{2,1}-2_{2,0}$, $3_{2,2}-2_{2,1}$, $3_{1,3}-2_{1,2}$, $3_{0,3}-2_{0,2}$ and $D_2CO$ $3_{0,3}-2_{0,2}$ observed toward AFGL5142, IRAS 05358+3543, and G5.89-0.39 using the IRAM 30 m telescope (Fontani et al. 2011, 2015) and the APEX SEPIA Band 5 receiver (this work). Red and blue lines indicate the fitted different velocity components for AFGL5142 and G5.89-0.39 with fixed velocity and width. The $C^{13}CS$ $N = 15-14$ and $J = 15-14$ transition is shown in the *fourth panels from the top*.

**Table A.1.** Transitions of $H_2CO$, $H_2^{13}CO$, HDCO, and $D_2CO$ observed with APEX SEPIA and the IRAM-30 m telescope.

| Species | Transition | Frequency [GHz] | $E_{up}$ [K] | $A_{ij}$ [$s^{-1}$] | Telescope |
|---|---|---|---|---|---|
| $D_2CO$ | $3_{0,3} \rightarrow 2_{0,2}$ | 174.413 | 16.8 | 1.44e-04 | APEX |
| HDCO | $3_{1,3} \rightarrow 2_{1,2}$ | 185.307 | 25.8 | 1.53e-04 | APEX |
| HDCO | $3_{0,3} \rightarrow 2_{0,2}$ | 192.893 | 18.5 | 1.94e-04 | APEX |
| HDCO | $3_{2,2} \rightarrow 2_{2,1}$ | 193.392 | 50.4 | 1.09e-04 | APEX |
| HDCO | $3_{2,1} \rightarrow 2_{2,0}$ | 193.907 | 50.4 | 1.10e-04 | APEX |
| $H_2^{13}CO$ | $3_{1,3} \rightarrow 2_{1,2}$ | 206.131 | 31.6 | 2.11e-04 | APEX |
| $H_2CO$ | $9_{1,8} \rightarrow 9_{1,9}$ | 216.569 | 174.0 | 7.22e-06 | IRAM |
| $H_2CO$ | $3_{0,3} \rightarrow 2_{0,2}$ | 218.222 | 21.0 | 2.82e-04 | IRAM |
| $H_2CO$ | $3_{2,2} \rightarrow 2_{2,1}$ | 218.476 | 68.1 | 1.57e-04 | IRAM |
| $H_2CO$ | $3_{2,1} \rightarrow 2_{2,0}$ | 218.760 | 68.1 | 1.58e-04 | IRAM |

**Table A.2.** Fitted parameters of the observed $H_2CO$, $H_2^{13}CO$, HDCO, and $D_2CO$ lines.

| Line | Area [K km s$^{-1}$] | $v_{LSR}$ [km s$^{-1}$] | *FWHM* [km s$^{-1}$] | $T_{MB}$ [K] |
|---|---|---|---|---|
| | | **AFGL5142** | | |
| $D_2CO$ $3_{0,3}\rightarrow2_{0,2}$ | 0.13 (0.01) | **−3.66 (0.06)** | 1.3 (0.2) | 0.10 (0.01) |
| | 0.14 (0.01) | **−2.08 (0.05)** | 1.4 (0.3) | 0.09 (0.01) |
| HDCO $3_{0,3}\rightarrow2_{0,2}$ | 0.45 (0.01) | −3.66 | 1.3 | 0.34 (0.01) |
| | 0.52 (0.01) | −2.08 | 1.4 | 0.35 (0.01) |
| HDCO $3_{1,3}\rightarrow2_{1,2}$ | 0.44 (0.04) | −3.66 | 1.3 | 0.33 (0.04) |
| | 0.51 (0.04) | −2.08 | 1.4 | 0.34 (0.04) |
| HDCO $3_{2,2}\rightarrow2_{2,1}$ | 0.07 (0.06) | −3.66 | 1.3 | 〃 0.06 (0.01) |
| | 0.10 (0.06) | −2.08 | 1.4 | 0.07 (0.01) |
| HDCO $3_{2,1}\rightarrow2_{2,0}$ | 0.07 (0.01) | −3.66 | 1.3 | 0.06 (0.01) |
| | 0.09 (0.01) | −2.08 | 1.4 | 0.06 (0.01) |
| $H_2^{13}CO$ $3_{1,2}\rightarrow2_{1,2}$ | 0.35 (0.01) | −3.66 | 1.3 | 0.26 (0.01) |
| | 0.38 (0.01) | −2.08 | 1.4 | 0.25 (0.01) |
| $H_2CO$ $3_{0,3}\rightarrow2_{0,2}$ | 8.81 (0.48) | −3.66 | 1.3 | 6.60 (0.48) |
| | 9.62 (0.51) | −2.08 | 1.4 | 6.47 (0.48) |
| | | **IRAS 05358+3543** | | |
| $D_2CO$ $3_{0,3}\rightarrow2_{0,2}$ | 0.12 (0.01) | −16.49 (0.15) | 2.6 (0.4) | 0.04 (0.01) |
| HDCO $3_{0,3}\rightarrow2_{0,2}$ | 0.57 (0.01) | −16.49 | 2.6 | 0.21 (0.01) |
| HDCO $3_{1,3}\rightarrow2_{1,2}$ | 0.64 (0.05) | −16.49 | 2.6 | 0.23 (0.04) |
| HDCO $3_{2,2}\rightarrow2_{2,1}$ | 0.08 (0.04) | −16.49 | 2.6 | 0.03 (0.01) |
| HDCO $3_{2,1}\rightarrow2_{2,0}$ | 0.07 (0.01) | −16.49 | 2.6 | 0.03 (0.01) |
| $H_2^{13}CO$ $3_{1,2}\rightarrow2_{1,2}$ | 0.45 (0.01) | −16.49 | 2.6 | 0.16 (0.01) |
| $H_2CO$ $3_{0,3}\rightarrow2_{0,2}$ | 13.70 (0.14) | −16.49 | 2.6 | 4.95 (0.09) |
| | | **G5.89-0.39** | | |
| $D_2CO$ $3_{0,3}\rightarrow2_{0,2}$ | ≤0.03 | ... | ... | ≤0.02 |
| HDCO $3_{0,3}\rightarrow2_{0,2}$ | 0.84(0.03) | 8.37(0.08) | 3.60 (0.18) | 0.22 (0.01) |
| | 0.19(0.02) | 11.70 (0.08) | 1.60 (0.21) | 0.11 (0.01) |
| HDCO $3_{1,3}\rightarrow2_{1,2}$ | 0.73(0.03) | 8.37 | 3.6 | 0.19 (0.01) |
| | 0.19(0.02) | 11.7 | 1.6 | 0.11 (0.01) |
| HDCO $3_{2,2}\rightarrow2_{2,1}$ | 0.18(0.11) | 8.37 | 3.6 | 0.05 (0.01) |
| | 0.11(0.08) | 11.7 | 1.6 | 0.06 (0.01) |
| HDCO $3_{2,1}\rightarrow2_{2,0}$ | 0.21(0.03) | 8.37 | 3.6 | 0.05 (0.01) |
| | 0.07(0.01) | 11.7 | 1.6 | 0.04 (0.01) |
| $H_2^{13}CO$ $3_{1,2}\rightarrow2_{1,2}$ | 1.87 (0.03) | 8.37 | 3.6 | 0.48 (0.02) |
| | 0.39 (0.02) | 11.7 | 1.6 | 0.23 (0.02) |
| $H_2CO$ $3_{0,3}\rightarrow2_{0,2}$ | 50.03(1.61) | 8.37 | 3.6 | 13.05 (0.93) |
| | 15.16(1.07) | 11.7 | 1.6 | 8.90 (0.93) |

**Notes.** Errors in peak intensity correspond to the 1$\sigma$ rms level in the spectra. For the HDCO, $H_2^{13}CO$, and $H_2CO$ spectra of AFGL5142 and IRAS 05358+3543, we fitted the $v_{LSR}$ and FWHM values based on the $D_2CO$ velocity components. For G5.89-0.39, we derived the velocity and width of the two components based on the HDCO $3_{0,3} \rightarrow 2_{0,2}$ line.